ISSN: 1410-8917
Jurnal Kimia Sains & Aplikasi
e-ISSN: 2597-9914

Jurnal Kimia Sains dan Aplikasi 28 (4) (2025): 168-175
Jurnal Kimia Sains dan Aplikasi
Journal of Scientific and Applied Chemistry
Journal homepage: http://ejournal.undip.ac.id/index.php/ksa

Impact of Modifying Filler into Porous on Hydrophobicity Behaviour of the Silica-HDPE Composite

Muhammad Defrizal [1], Tetty Kemala [1,*], Mohammad Khotib [1,2]

[1] Department of Chemistry, Faculty of Mathematics and Natural Science, Bogor Agricultural University, Bogor, Indonesia
[2] Integrated Laboratory, Bogor Agricultural University, Bogor, Indonesia

* Corresponding author: tettykemala@apps.ipb.ac.id

https://doi.org/10.14710/jksa.28.4.168-175

Article Info

Article history:

Received: 01st June 2024
Revised: 14th March 2025
Accepted: 08th April 2025
Online: 31st May 2025

Keywords:
Cassie-Baxter equation; hydrophobicity; porous filler; silica-HDPE composite; surface roughness

Abstract

Even though the approach is relatively simple and does not require additional treatment, the porous filler method has not been widely utilized to boost the composite's hydrophobicity. Therefore, this study wants to show that silica's porosity as a filler material affects the surface roughness and hydrophobicity of its composite (in this case, silica-HDPE). Pore formation in silica uses the soft-template method with Tween-80 as the mould. The amount of surfactant was varied by 0, 5, and 10 g. The particles are then physically composited into the HDPE matrix. Surface characterization of silica particles analyzed by Brunauer-Emmett-Teller (BET) shows enhancement in particle porosity as the amount of surfactant added is increased. When it is inserted into HDPE, the silica particles with the highest porosity have the greatest surface roughness. It is confirmed by the wavy surface texture of this composite when it is characterized using an Atomic Force Microscope (AFM). These results are accompanied by a significant enhancement in the contact angle value at each concentration. From the contact angle and AFM data, porous silica has the role of surface texture provider in raising its roughness. It affects the improvement of the hydrophobicity according to the Cassie-Baxter equation, which states that the more air fraction formed on a surface, the higher the contact angle obtained.

1. Introduction

Superhydrophobic is a surface property that can repel water, as well as has a contact angle greater than 150° and a hysterical contact angle of less than 10° [1]. This value is inseparable from its rough surface texture and low surface energy [2]. The superhydrophobic surface has been widely applied in various ways, namely as a self-cleaning [3], anti-corrosive [4], anti-blood adsorption [5], and anti-freezing [6]. Most of those applications imitate the pattern of the surface leaves in nature microscopically. For instance, Xu *et al.* [7] tried to create a superhydrophobic coating from Ag nanoparticles-polydopamine to be applied for oil/water separation and self-cleaning by mimicking the surface of the lotus leaf.

The hydrophobicity of a surface can be increased by elevating the roughness and decreasing the surface energy. This method can be acquired by compositing the two materials, each of which has those properties. Various studies have proven this. Lu *et al.* [8] in their research showed an increase in the value of the contact angle of the silica-silicone sealant composite when silica was added to the polymer matrix, namely from 112.5° (without adding silica) to 169.8° (with the addition of 2% silica (w/w)). It was due to the rising surface roughness from 1.94 nm (only the silicone-sealant matrix) to 63.7 nm (2% (w/w) addition of silica). Similar results were also obtained from the study of Bahgat Radwan *et al.* [9], who showed enlargement in surface roughness and contact angle when Al_2O_3 was appended to the polystyrene matrix.

Based on the Cassie-Baxter theory, the surface hydrophobicity rises if the number of solid fractions is reduced. Therefore, pore formation is one thing that needs to be considered in fabricating composites with higher contact angles. Pores in the composite surface can be carried out using a variety of methods, including adding an additive substance when electrospinning [10], plasma treatment [11], and nonsolvent-induced phase separation (NIPS) [12, 13, 14]. However, those methods have several weaknesses, which include needing a sophisticated instrument, requiring additional treatment, and lacking transparency. Therefore, another approach is needed to overcome some of these weaknesses, one of which is forming porous filler material.

The porous filler material has not been a concern in manufacturing superhydrophobic composites. In reality, this approach has several advantages, including not requiring modification of the chemical structure to become hydrophobic, as in a study conducted by Suyambulingam *et al.* [15] and Wang *et al.* [16]; not considering the other physical parameters, like research done by Pawar *et al.* [17]; as well as being more transparent [18]. Therefore, this study wants to prove that forming porous filler materials in composites can accelerate their hydrophobicity.

In this study, silica was used as the filler material to introduce porosity on the particle surface. Porous silica is rarely employed to generate surface roughness aimed at enhancing the hydrophobicity of a composite, as it is more commonly utilized in biological applications such as drug delivery and therapeutic agents [19, 20]. Pore formation was achieved through a soft-templating method [21], using Tween-80 as the templating agent. Tween-80 was selected due to its low tendency to agglomerate, uniform spherical morphology, and smaller particle size compared to other surfactants such as cetyltrimethylammonium bromide (CTAB) and sodium dodecyl sulfate (SDS) [22]. The amount of surfactant was varied (0, 5, and 10 g) to investigate the effect of silica particle porosity on the hydrophobicity of the resulting composite.

The synthesized porous silica particles were then dispersed in a high-density polyethylene (HDPE) solution, which served as the matrix to reduce the surface energy of the composite. It is important to note that the hydroxyl (-OH) groups on the silica surface were not chemically modified to become hydrophobic; therefore, the composite's hydrophobicity was solely influenced by the pore structure. Fabrication results showed that composites containing silica particles with higher porosity exhibited increased water contact angle values, indicating enhanced hydrophobicity. This was further supported by an increase in surface roughness, suggesting that porous silica contributes to the surface texture prior to HDPE coating.

2. Experimental

2.1. Materials and Instrumentations

HDPE ore was purchased on Lotte Titanvene with of 18 g/min melt flow index. Sodium silicate (Na_2SiO_3) and Tween-80 (98% purity, Merck Milipore) had already been obtained in the Integrated Laboratory at Bogor Agricultural University. Absolute ethanol, acetone, and xylene, with a purity of 95%, 99.8%, and 99%, respectively, were supplied from Merck Milipore. The instruments used to characterize both silica particles and their composites were Scanning Electron Microscope (SEM; Thermo Scientific), X-ray diffraction (XRD; Rigaku Minifex), Atomic Force Microscopy (AFM; Bruker Nanoscan), Brunauer-Emmett-Teller (BET; Quantachrome NovaWin Instrument), Fourier Transform Infrared (FTIR; Shimadzu IRPrestige-21), cellular phone's camera (Xiaomi, Redmi Note 5), and laptop (Apple, MacBook Pro) installed ImageJ software (version 1.53k, National Institutes of Health).

2.2. Synthesis of Silica from Sodium Silicate

Several aliquots of 0.88 mL glacial acetic acid were each dissolved in 20 mL of distilled water. Subsequently, 5.0185 g and 10.0196 g of Tween-80 were added to the acetic acid solutions and stirred until fully dissolved. As a control, silica synthesis without the addition of Tween-80 was also conducted. In parallel, 7.43 wt% of Na_2SiO_3 was dissolved in 20 mL of distilled water in separate beakers. The Na_2SiO_3 solution was then slowly added along the walls of the container into the Tween–80–acetic acid mixtures under continuous stirring using a magnetic stir bar. The resulting mixtures were sonicated at 80 kHz for 2 hours to promote the formation of silica particles.

The precipitate formed in the Tween-80-containing mixtures was separated by centrifugation. In contrast, the mixture without Tween-80, which did not form a precipitate, was processed by freeze-drying. The collected precipitate was washed with distilled water until a neutral pH was achieved, then oven-dried at 110°C until constant weight, and finally calcined in a furnace at 550°C for 2 hours. The resulting silica particles synthesized with 0, 5, and 10 g of Tween-80 were designated as PS 0, PS 5, and PS 10, respectively.

2.3. Fabrication of Silica-HDPE Composite

Before fabricating the composite, the glass substrate was first prepared. It was cleaned thoroughly with distilled water, followed by acetone. The coating area on the glass substrate was defined with dimensions of 6.5 × 1.5 cm, and the uncoated portions were masked using black duct tape. Once the substrate preparation was complete, the silica–HDPE composite fabrication process began.

A solution of 1.16 wt% HDPE ore was prepared by dissolving it in 10 mL of xylene, which was heated on a hot plate at 120°C until the HDPE was fully dissolved. Silica particles, obtained from the previous treatments, were then added at concentrations of 5%, 10%, 15%, and 20% by weight relative to HDPE (w/w), and mixed under the same temperature conditions for 2 minutes. These concentrations were selected to evaluate the effect and trend of incorporating small amounts of silica on the composite's hydrophobicity.

The resulting mixture was coated onto the prepared glass substrate using the solution casting method. The coated samples were then left to dry at room temperature for 24 hours to allow solvent evaporation. The resulting composites, incorporating PS 0, PS 5, and PS 10 as fillers, were designated as PS-H 0, PS-H 5, and PS-H 10, respectively.

2.4. Characterization of Silica Particles and Silica-HDPE Composites

The morphologies of silica particles and silica-HDPE composites were characterized using SEM with back-scattered electrons (BSE) as the electron source. Imaging was conducted at an accelerating voltage of 10 kV and a chamber pressure of 1 Pa. The analysis focused on particle size and shape for the silica samples, and surface distribution for the composites. The pores in the silica particles were analyzed using a BET with nitrogen gas (N_2) as an adsorbate. The parameters evaluated included surface area, total pore volume (porosity), and average pore diameter. Pore size distribution, as influenced by varying amounts of surfactant, was determined using the Barrett–Joyner–Halenda (BJH) method [23].

The crystallinity of the silica particles due to adding Tween-80 as a template was determined using XRD. The instrument operated at a wavelength of 1.54 nm, with scans conducted over a 3–90° 2θ range and a step size of 0.02°. Functional groups present in the silica particles and their composites were identified using Fourier-transform infrared (FTIR) spectroscopy with KBr pellets as the background. Lastly, the surface roughness of the silica–HDPE composites was measured using atomic force microscopy (AFM) in non-contact mode.

2.5. Contact Angle Measurement

Each droplet was then photographed from a distance of 5 cm to clearly capture the phase boundary between the liquid and the solid (composite surface). The droplet images were analyzed using ImageJ software. Contact angle measurements were performed using the curve fitting method, where the experimentally observed droplet shape was fitted to a theoretical projection, either circular or elliptical. The water contact angle was determined based on the projection yielding the lowest standard deviation value, indicating the best fit.

3. Results and Discussion

3.1. Characteristics of The Synthesized Silica

The morphological differences between silica particles synthesized with and without Tween-80 surfactant are shown in Figure 1. As observed in Figure 1a, most silica particles synthesized in the presence of Tween-80 are spherical, with diameters ranging from 0.76 to 2.22 μm, indicating a high degree of polydispersity. This high polydispersity is attributed to the use of polar solvents. According to Malay *et al.* [24], the polydispersity of silica particles increases with the polarity of the solvent. Additionally, hydrogen bonding interactions between Tween-80 and sodium silicate influence the morphology of the resulting silica particles by accelerating the incorporation of silicate ions from the solution into the growing silica network. However, this process may be hindered at higher surfactant concentrations [25, 26]. In contrast, in the absence of surfactant, the silica formation reaction proceeds more slowly, resulting in poorly defined or indistinct particle morphologies, as seen in Figure 1b.

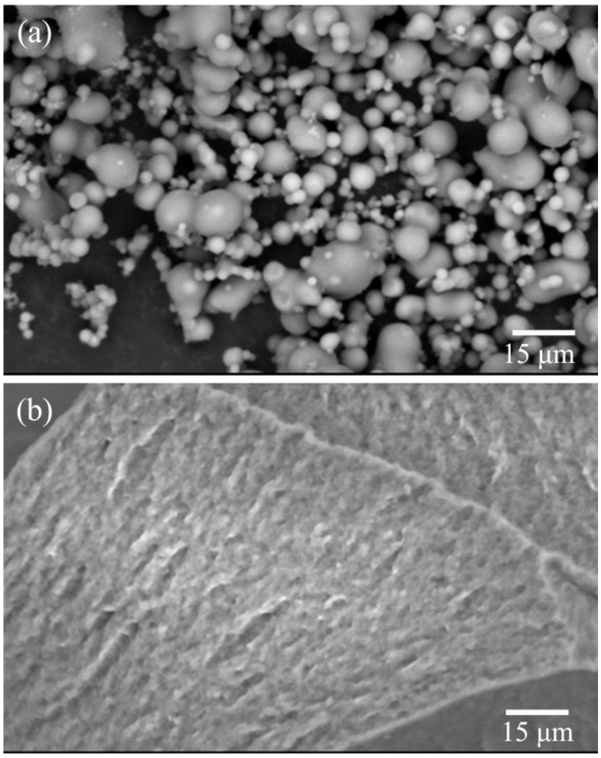

Figure 1. Morphology of silica particles synthesized (a) with and (b) without the addition of Tween-80 surfactant

The differences in surface area and pore volume of silica particles synthesized with varying amounts of Tween-80 can be observed from the nitrogen adsorption–desorption isotherm curves shown in Figure 2. As illustrated, the isotherms for PS 0 and PS 5 correspond to type IV, while PS 10 exhibits a type III isotherm. This variation in isotherm type indicates that PS 10 possesses a higher total pore volume compared to PS 0 and PS 5, as summarized in Table 1. Moreover, the shape of the PS 10 curve suggests the presence of surface cavities or hollow structures, which is consistent with the isotherm profiles reported by Zea *et al.* [27] and Hadipour Moghaddam *et al.* [28] during the synthesis of hollow porous silica nanoparticles.

As a result, the specific surface area of PS 10 is lower than that of PS 5 and PS 0 (Table 1). The increase in surface area observed in PS 0 and PS 5 is attributed to the formation of Tween-80 micelles, which are uniformly dispersed in the solution and serve as soft templates for pore formation. However, when the concentration of Tween-80 reaches approximately 10 g, the micelles grow in size, leading to the development of larger voids or hollow structures within the particles.

Table 1. Characteristics of the pores in the silica particles obtained from the treatment of surfactant addition

Sample	Surface area (m^2/g)	Total pore volume (mL/g)	Pore diameter (Å)
PS 0	407.776	0.2875	17.000
PS 5	633.539	0.4358	21.702
PS 10	391.232	1.375	39.362

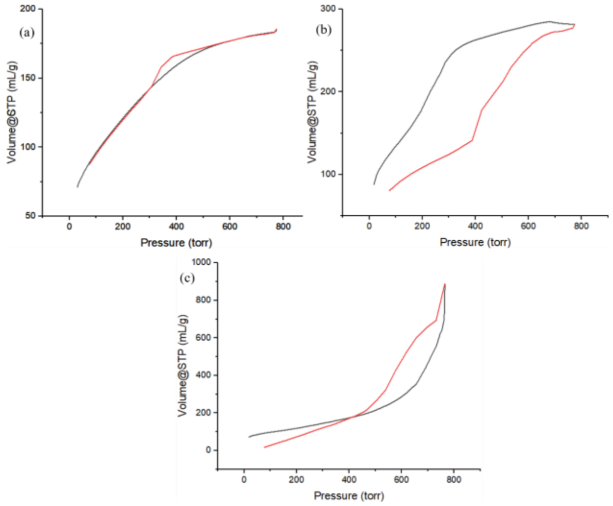

Figure 2. Nitrogen adsorption–desorption isotherms of (a) PS 0, (b) PS 5, and (c) PS 10. The black line represents the adsorption branch, while the red line indicates the desorption branch

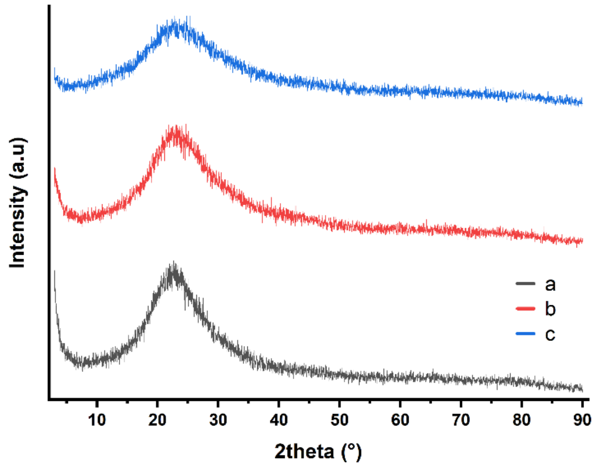

Figure 3. XRD patterns of silica particles synthesized with varying amounts of Tween-80 surfactant: (a) PS 10, (b) PS 5, and (c) PS 0

Differences in crystallinity among PS 0, PS 5, and PS 10 are shown in the XRD patterns in Figure 3. All synthesized silica particles exhibit amorphous characteristics, as indicated by the broad diffraction peaks across all treatments. This amorphous nature is associated with the formation of pores on the particle surfaces. However, with increasing amounts of Tween-80, the peaks become sharper and more distinct, suggesting a slight improvement in crystallinity.

This trend is further supported by the decreasing full-width at half maximum (FWHM) values: 14.68 for PS 0, 11.43 for PS 5, and 9.86 for PS 10. The reduction in FWHM indicates a gradual improvement in the ordering of the silica network. The narrower diffraction peaks imply an increased proportion of cristobalite phase in the silica composition (Table 2). These findings indicate that the presence of Tween-80 not only facilitates pore formation but also promotes a more ordered structural arrangement. Acting as a structure-directing agent, the surfactant guides the organization of silicate units during synthesis [29], thereby enhancing the crystallinity of the resulting silica particles.

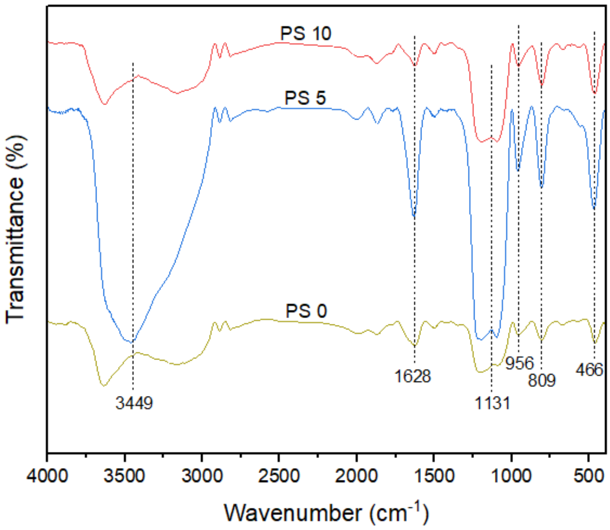

Figure 4. FTIR spectra of the synthesized silica

Table 2. Crystalline composition of silica particles synthesized with varying amounts of Tween-80

Silica particle	Crystal composition (%)		
	Quartz	Tridymite	Crystobalite
PS 0	13.9	78.3	7.8
PS 5	11.1	39.7	49.2
PS 10	3.3	31.5	65.1

The functional groups present in silica particles synthesized with varying amounts of Tween-80 are shown in Figure 4. The results indicate that all synthesized silica particles possess -OH groups on their surfaces, as evidenced by the stretching vibration observed between 3500 and 3000 cm^{-1} and the bending vibration at 1628 cm^{-1} [30, 31]. These characteristic peaks suggest that the silica particles are hydrophilic in nature. Additional bonds present on the silica surface include Si-O-Si stretching vibrations (asymmetric at 1131 cm^{-1}, symmetric at 809 cm^{-1}, and bending at 466 cm^{-1}) and Si-O-H stretching at 956 cm^{-1} [32].

3.2. Surface Characteristics of Silica-HDPE Composite

The functional groups present on the surface of the silica–HDPE composite are identified in Figure 5. The spectrum reveals the presence of $-CH_2-$ (1487 cm^{-1}), $-CH_3$ (1366 cm^{-1}), and -CH (2863 cm^{-1}) stretching vibrations, indicating the presence of HDPE. Additionally, characteristic silica-related vibrations are observed, including Si-O-Si asymmetric stretching (1088 cm^{-1}), symmetric stretching (805 cm^{-1}), and bending (467 cm^{-1}), as well as Si-O-H stretching at 962 cm^{-1}. The -OH group is also detected with a broad stretching peak between 3500 and 3000 cm^{-1} and a bending vibration at 1698 cm^{-1}. These results suggest that, despite varying surfactant concentrations, the silica particles form physical interactions with HDPE, as evidenced by the lack of new functional groups, indicating no significant chemical bonding between the two components.

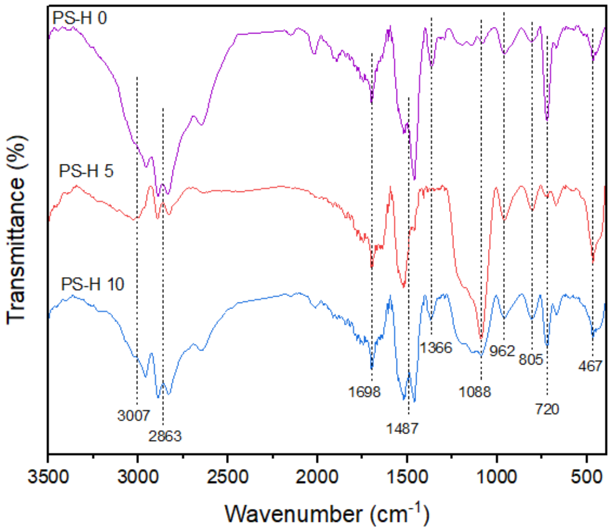

Figure 5. FTIR spectra of silica-HDPE composite

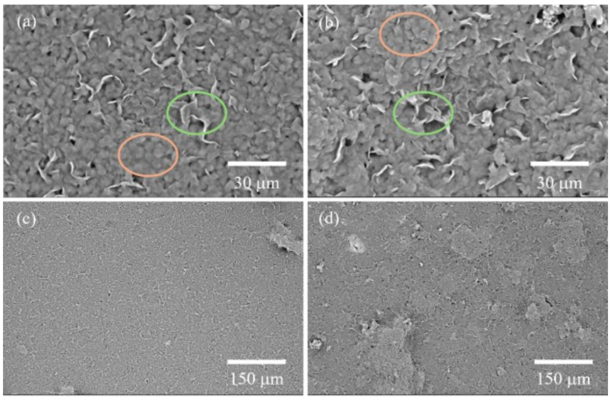

Figure 6. Surface morphology of silica-HDPE composites: (a, c) without and (b, d) with the addition of Tween-80 surfactant at different magnifications

Figure 6 shows the surface characteristics of silica–HDPE composites, both without and with Tween-80 surfactant. In the images, HDPE (green circle) forms a top layer that coats the underlying silica particles (orange circle) (Figure 6a and b). These observations suggest that the hydroxyl groups on the silica particles are covered by the HDPE layer, thereby reducing the surface energy of the silica–HDPE composite. Additionally, the silica particles are uniformly distributed within the HDPE matrix. At lower magnifications (Figure 6c and d), the composite containing surfactant shows more pronounced pores and a wavier texture compared to the composite without surfactants.

3.3. Hydrophobicity and Surface Texture of Silica-HDPE Composites Due to Filler Porosity Variations

Figure 7 illustrates the trend of water contact angle values for silica–HDPE composites at varying filler concentrations and porosity levels, based on the average of three measurements. An increase in water contact angle is observed across all silica particles' porosity levels as the filler concentration increases. As the distance between silica particles decreases, the contact angle rises. However, at 15% (w/w) concentration, the contact angle slightly decreases, attributed to a reduced air fraction on the composite surface. Additionally, the rise in –OH groups and uneven filler distribution in the HDPE matrix contribute to greater variation in contact angle measurements for non-porous silica, especially at 5–15% (w/w), compared to the more stable results observed with porous silica particles.

This graph further demonstrates that increasing the porosity of silica particles enhances their hydrophobicity. This can be explained using the Cassie-Baxter equation (Equations 1 and 2), which predicts that the contact angle (θ_e^r) increases when the air fraction (f_a) is higher and the solid fraction (f_s) is lower [29]. Therefore, the formation of pores in the silica particles increases the air fraction on the surface, thereby improving the hydrophobicity.

$$\theta_e^r = f_s(\cos\theta_s + 1) - 1 \tag{1}$$

$$f_s = 1 - f_a \tag{2}$$

The surface roughness contributes to the enhancement of the contact angle, influenced by the increasing porosity of silica particles. Figure 8 presents the surface contours of silica–HDPE composites with different filler porosity levels. In PS-H 0, the surface is relatively flat, as most of the area is concentrated around the z-axis value of 0 (Figure 8a). With the addition of 5 g of Tween-80, the silica becomes more porous, and the composite surface exhibits a wavelike contour (Figure 8b), marked by a narrower yellow region representing areas above the z-axis. This wavy texture becomes more pronounced in PS 10 (Figure 8c), indicating further increases in surface irregularities. The growing waviness with higher silica porosity suggests an increase in surface roughness. This is further supported by the significant rise in the average surface roughness (Sa) values observed from PS-H 0 to PS-H 10.

The characterization results presented in Figure 8 indicate that the texture of the silica–HDPE composite surface closely follows the contour of its filler material. As illustrated in Figure 9, the silica particles serve as structural templates that shape the surface texture of the composite before being encapsulated by the HDPE matrix. Silica particles with high porosity exhibit wavy surface contours due to the presence of numerous air voids or pores. When incorporated into the HDPE matrix, these contours result in a rough composite surface and, consequently, increased hydrophobicity. Conversely, silica particles with low or no porosity exhibit relatively flat contours, yielding a smoother composite surface with lower hydrophobicity.

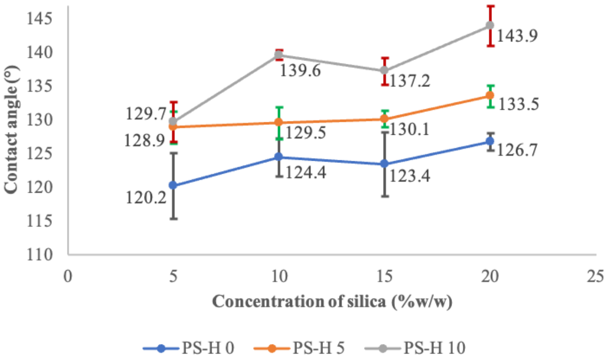

Figure 7. Contact angle values of silica-HDPE composites at various concentrations

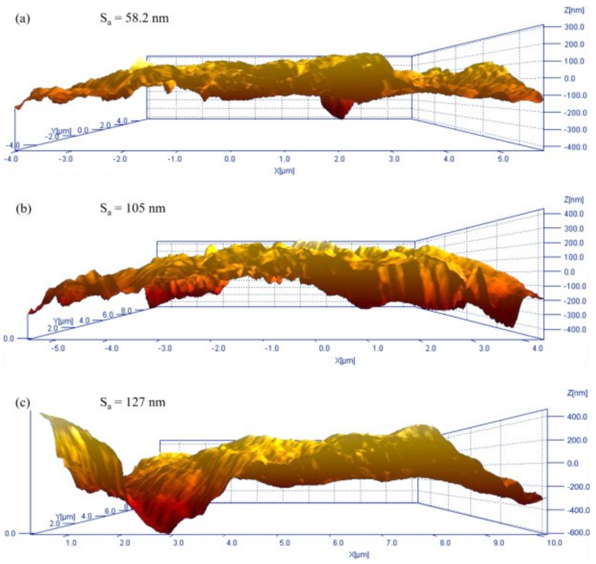

Figure 8. Surface topography of silica-HDPE composites containing 20% (w/w) silica: (a) PS-H 0, (b) PS-H 5, and (c) PS-H 10

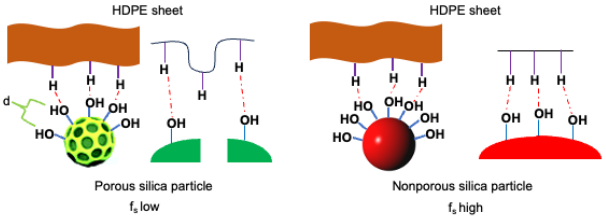

Figure 9. Illustration of the physical interaction between silica particles and HDPE matrix at different silica porosities

In addition to porosity, the surface characteristics of the composite are also influenced by the number of hydroxyl (-OH) groups present on the silica surface and their interaction with HDPE. Porous silica contains fewer -OH groups, and the distance (d) between them is greater compared to nonporous silica. As a result, some methyl (- CH_3) groups from HDPE that do not interact with -OH groups conform to the pore structures of the silica filler. This contributes to surface curvature, thereby increasing both surface roughness and hydrophobicity of the composite.

This study demonstrates that modifying silica particles to increase their porosity effectively enhances the hydrophobicity of the resulting silica–HDPE composite. This approach is relatively straightforward and does not require controlling additional physical parameters, such as the thickness of the composite film, to attain high hydrophobic performance [17]. Furthermore, it eliminates the need for post-treatment steps, such as the use of non-solvents to induce surface porosity [14], or chemical modification of the silica particles' functional groups, as carried out in the study by Wang *et al.* [16].

4. Conclusion

The synthesis of the silica–HDPE composite by increasing the porosity of the filler material has been proven effective in enhancing the composite's hydrophobicity across all concentrations. The PS-H 10 sample exhibited the highest contact angle and surface roughness at the greatest filler concentration, reaching 143.90 ± 2.97° and 127 nm, respectively. This is attributed to the role of porous silica particles, which serve as surface texture modifiers in the composite. When HDPE covers the silica filler, the resulting surface contour mimics the texture established by the silica particles. Highly porous silica produces a more pronounced wavy surface compared to less porous or nonporous particles, thereby significantly increasing surface roughness. Moreover, the increased porosity contributes to a greater air fraction and a reduced solid fraction at the composite surface, which enhances hydrophobicity in accordance with the Cassie–Baxter equation. In addition, higher porosity reduces the number of surface hydroxyl groups on silica, lowering the surface energy of the composite. This method is relatively straightforward and does not require additional treatments or the adjustment of other physical parameters to achieve enhanced hydrophobicity.

Acknowledgments

We would like to express our gratitude to the Ministry of Education, Culture, Research, and Technology of the Republic of Indonesia for funding this research through Grant Agreement No. 3866/IT3.L1/PT.01.03/P/B/2022.

References

[1] Jeya Jeevahan, M. Chandrasekaran, G. Britto Joseph, R. B. Durairaj, G. Mageshwaran, Superhydrophobic surfaces: a review on fundamentals, applications, and challenges, *Journal of Coatings Technology and Research*, 15, 2, (2018), 231-250 https://doi.org/10.1007/s11998-017-0011-x

[2] Yun-Yun Quan, Zhong Chen, Yuekun Lai, Zu-Sheng Huang, Huaqiong Li, Recent advances in fabricating durable superhydrophobic surfaces: a review in the aspects of structures and materials, *Materials Chemistry Frontiers*, 5, 4, (2021), 1655-1682 https://doi.org/10.1039/d0qm00485e

[3] Divya Kumar, Lin Li, Zhong Chen, Mechanically robust polyvinylidene fluoride (PVDF) based superhydrophobic coatings for self-cleaning applications, *Progress in Organic Coatings*, 101, (2016), 385-390 https://doi.org/10.1016/j.porgcoat.2016.09.003

[4] Bo Wang, Hongtao Liu, Chao Chen, Huaqiu Zhang, Chunchun Du, Lizao Zhou, Facile preparation of TPE/SiO_2 flexible superhydrophobic composite film with acid corrosion resistance and stretchable recyclability, *Materials Today Communications*, 25, (2020), 101318 https://doi.org/10.1016/j.mtcomm.2020.101318

[5] Nusret Celik, Furkan Sahin, Mahmut Ruzi, Mehmet Yay, Ekrem Unal, M. Serdar Onses, Blood repellent superhydrophobic surfaces constructed from nanoparticle-free and biocompatible materials, *Colloids and Surfaces B: Biointerfaces*, 205, (2021), 111864 https://doi.org/10.1016/j.colsurfb.2021.111864

[6] Tianxue Zhu, Yan Cheng, Jianying Huang, Jiaqing Xiong, Mingzheng Ge, Jiajun Mao, Zekun Liu, Xiuli Dong, Zhong Chen, Yuekun Lai, A transparent superhydrophobic coating with mechanochemical robustness for anti-icing, photocatalysis and self-

cleaning, *Chemical Engineering Journal*, 399, (2020), 125746 https://doi.org/10.1016/j.cej.2020.125746

[7] Zhanglian Xu, Koji Miyazaki, Teruo Hori, Fabrication of polydopamine-coated superhydrophobic fabrics for oil/water separation and self-cleaning, *Applied Surface Science*, 370, (2016), 243-251 https://doi.org/10.1016/j.apsusc.2016.02.135

[8] Zhenzhen Lu, Lijie Xu, Yang He, Jianting Zhou, One-step facile route to fabricate functionalized nano-silica and silicone sealant based transparent superhydrophobic coating, *Thin Solid Films*, 692, (2019), 137560 https://doi.org/10.1016/j.tsf.2019.137560

[9] Ahmed Bahgat Radwan, Aboubakr M. Abdullah, Adel M. A. Mohamed, Mariam A. Al-Maadeed, New Electrospun Polystyrene/Al_2O_3 Nanocomposite Superhydrophobic Coatings; Synthesis, Characterization, and Application, *Coatings*, 8, 2, (2018), 65 https://doi.org/10.3390/coatings8020065

[10] Yuan Liao, Chun-Heng Loh, Rong Wang, Anthony G. Fane, Electrospun Superhydrophobic Membranes with Unique Structures for Membrane Distillation, *ACS Applied Materials & Interfaces*, 6, 18, (2014), 16035-16048 https://doi.org/10.1021/am503968n

[11] Ramón Jiménez-Robles, Marta Izquierdo, Vicente Martínez-Soria, Laura Martí, Alicia Monleón, José David Badia, Stability of Superhydrophobicity and Structure of PVDF Membranes Treated by Vacuum Oxygen Plasma and Organofluorosilanisation, *Membranes*, 13, 3, (2023), 314 https://doi.org/10.3390/membranes13030314

[12] M. Satapathy, P. Varshney, D. Nanda, S. S. Mohapatra, A. Behera, A. Kumar, Fabrication of durable porous and non-porous superhydrophobic LLDPE/SiO_2 nanoparticles coatings with excellent self-cleaning property, *Surface and Coatings Technology*, 341, (2018), 31-39 https://doi.org/10.1016/j.surfcoat.2017.07.025

[13] Yuwei Zhu, Lei Pei, Jaweria Ambreen, Chuanxin He, To Ngai, Facile Preparation of a Fluorine-Free, Robust, Superhydrophobic Coating through Dip Coating Combined with Non-Solvent Induced Phase Separation (Dip-Coating-NIPS) Method, *Macromolecular Chemistry and Physics*, 221, 7, (2020), 2000023 https://doi.org/10.1002/macp.202000023

[14] Lingqi Zhong, Xiao Gong, Phase separation-induced superhydrophobic polylactic acid films, *Soft Matter*, 15, 46, (2019), 9500-9506 https://doi.org/10.1039/c9sm01624d

[15] Gokul Raja Thangaiyanadar Suyambulingam, Kadarkaraithangam Jeyasubramanian, Vimal Kumar Mariappan, Pandiyarasan Veluswamy, Hiroya Ikeda, Karthikeyan Krishnamoorthy, Excellent floating and load bearing properties of superhydrophobic ZnO/copper stearate nanocoating, *Chemical Engineering Journal*, 320, (2017), 468-477 https://doi.org/10.1016/j.cej.2017.03.052

[16] Peng Wang, Bo Sun, Tao Yao, Mingji Chen, Xiaoliang Fan, Huilong Han, Lin Li, Chao Wang, A novel dissolution and resolidification method for preparing robust superhydrophobic polystyrene/silica composite, *Chemical Engineering Journal*, 326, (2017), 1066-1073 https://doi.org/10.1016/j.cej.2017.06.058

[17] Popat G. Pawar, Ruimin Xing, Rahul C. Kambale, A. Madhan Kumar, Shanhu Liu, Sanjay S. Latthe, Polystyrene assisted superhydrophobic silica coatings with surface protection and self-cleaning approach, *Progress in Organic Coatings*, 105, (2017), 235-244 https://doi.org/10.1016/j.porgcoat.2017.01.016

[18] Norbert J. Janowicz, Hangtong Li, Frances L. Heale, Ivan P. Parkin, Ioannis Papakonstantinou, Manish K. Tiwari, Claire J. Carmalt, Fluorine-Free Transparent Superhydrophobic Nanocomposite Coatings from Mesoporous Silica, *Langmuir*, 36, 45, (2020), 13426-13438 https://doi.org/10.1021/acs.langmuir.0c01767

[19] Samira Jafari, Hossein Derakhshankhah, Loghman Alaei, Ali Fattahi, Behrang Shiri Varnamkhasti, Ali Akbar Saboury, Mesoporous silica nanoparticles for therapeutic/diagnostic applications, *Biomedicine & Pharmacotherapy*, 109, (2019), 1100-1111 https://doi.org/10.1016/j.biopha.2018.10.167

[20] Miguel Manzano, María Vallet-Regí, Mesoporous Silica Nanoparticles for Drug Delivery, *Advanced Functional Materials*, 30, 2, (2020), 1902634 https://doi.org/10.1002/adfm.201902634

[21] Sunil Kumar, M. M. Malik, Rajesh Purohit, Synthesis Methods of Mesoporous Silica Materials, *Materials Today: Proceedings*, 4, 2, Part A, (2017), 350-357 https://doi.org/10.1016/j.matpr.2017.01.032

[22] Raju Kumar Sharma, Gobinda Dey, Pritam Banerjee, Jyoti Prakash Maity, Chung-Ming Lu, Shau-Chun Wang, Yi-Hsun Huang, Pin-Yun Lin, Yung-Ping Chen, Chien-Yen Chen, Influence of chemical and bio-surfactants on physiochemical properties in mesoporous silica nanoparticles synthesis, *Journal of Materials Research and Technology*, 24, (2023), 2629-2639 https://doi.org/10.1016/j.jmrt.2023.03.170

[23] Raoof Bardestani, Gregory S. Patience, Serge Kaliaguine, Experimental methods in chemical engineering: specific surface area and pore size distribution measurements—BET, BJH, and DFT, *The Canadian Journal of Chemical Engineering*, 97, 11, (2019), 2781-2791 https://doi.org/10.1002/cjce.23632

[24] Ozge Malay, Iskender Yilgor, Yusuf Z. Menceloglu, Effects of solvent on TEOS hydrolysis kinetics and silica particle size under basic conditions, *Journal of Sol-Gel Science and Technology*, 67, 2, (2013), 351-361 https://doi.org/10.1007/s10971-013-3088-4

[25] Fiona W. M. Ling, Hayder A. Abdulbari, Chin Sim-Yee, Investigating the effect of nonionic surfactant on the silica nanoparticles formation and morphology in a microfluidic reactor, *Journal of Flow Chemistry*, 11, 4, (2021), 737-750 https://doi.org/10.1007/s41981-021-00139-4

[26] Viktoriya Semeykina, Ilya Zharov, Medium controlled aggregative growth as a key step in mesoporous silica nanoparticle formation, *Journal of Colloid and Interface Science*, 615, (2022), 236-247 https://doi.org/10.1016/j.jcis.2022.01.166

[27] Cristina Zea, Jenifer Alcántara, Rosa Barranco-García, Manuel Morcillo, Daniel De la Fuente, Synthesis and Characterization of Hollow Mesoporous Silica Nanoparticles for Smart Corrosion Protection, *Nanomaterials*, 8, 7, (2018), 478 https://doi.org/10.3390/nano8070478

[28] Seyyed Pouya Hadipour Moghaddam, Mostafa Yazdimamaghani, Hamidreza Ghandehari, Glutathione-sensitive hollow mesoporous silica nanoparticles for controlled drug delivery, *Journal of Controlled Release*, 282, (2018), 62-75 https://doi.org/10.1016/j.jconrel.2018.04.032

[29] Mariya I. Vlasenkova, Dolinina Ekaterina S., Elena V. and Parfenyuk, Preparation of mesoporous silica microparticles by sol–gel/emulsion route for protein release, *Pharmaceutical Development and Technology*, 24, 2, (2019), 243-252 https://doi.org/10.1080/10837450.2018.1457051

[30] S. Saravanan, R. S. Dubey, Synthesis of SiO_2 nanoparticles by sol-gel method and their optical and structural properties, *Romanian Journal of Information Science and Technology*, 23, 1, (2020), 105-112

[31] Kamlesh Panwar, Manjeet Jassal, Ashwini K. Agrawal, In situ synthesis of Ag–SiO_2 Janus particles with epoxy functionality for textile applications, *Particuology*, 19, (2015), 107-112 https://doi.org/10.1016/j.partic.2014.06.007

[32] Dian Maruto Widjonarko, Jumina Jumina, Indriana Kartini, Nuryono Nuryono, Phosphonate Modified Silica for Adsorption of Co(II), Ni(II), Cu(II), and Zn(II), *Indonesian Journal of Chemistry*, 14, 2, (2014), 143-151